Effect of surface hydroxyl groups on heat capacity of mesoporous silica

Michal Marszewski, Danielle Butts, Esther Lan, Yan Yan, Sophia C. King, Patricia E. McNeil, Tiphaine Galy, Bruce Dunn, Sarah H. Tolbert, Yongjie Hu, and Laurent Pilon

Citation: Appl. Phys. Lett. **112**, 201903 (2018); doi: 10.1063/1.5027080
View online: https://doi.org/10.1063/1.5027080
View Table of Contents: http://aip.scitation.org/toc/apl/112/20
Published by the American Institute of Physics

Effect of surface hydroxyl groups on heat capacity of mesoporous silica

Michal Marszewski,[1] Danielle Butts,[2] Esther Lan,[2] Yan Yan,[3] Sophia C. King,[3] Patricia E. McNeil,[2] Tiphaine Galy,[1] Bruce Dunn,[2] Sarah H. Tolbert,[2,3] Yongjie Hu,[1] and Laurent Pilon[1,a)]

[1]*Mechanical and Aerospace Engineering Department, University of California, Los Angeles, Los Angeles, California 90095, USA*

[2]*Department of Materials Science and Engineering, University of California, Los Angeles, Los Angeles, California 90095, USA*

[3]*Department of Chemistry and Biochemistry, University of California at Los Angeles, Los Angeles, California 90095, USA*

(Received 27 February 2018; accepted 27 April 2018; published online 16 May 2018)

This paper quantifies the effect of surface hydroxyl groups on the effective specific and volumetric heat capacities of mesoporous silica. To achieve a wide range of structural diversity, mesoporous silica samples were synthesized by various methods, including (i) polymer-templated nanoparticle-based powders, (ii) polymer-templated sol-gel powders, and (iii) ambigel silica samples dried by solvent exchange at room temperature. Their effective specific heat capacity, specific surface area, and porosity were measured using differential scanning calorimetry and low-temperature nitrogen adsorption-desorption measurements. The experimentally measured specific heat capacity was larger than the conventional weight-fraction-weighted specific heat capacity of the air and silica constituents. The difference was attributed to the presence of OH groups in the large internal surface area. A thermodynamic model was developed based on surface energy considerations to account for the effect of surface OH groups on the specific and volumetric heat capacity. The model predictions fell within the experimental uncertainty. *Published by AIP Publishing*. https://doi.org/10.1063/1.5027080

Mesoporous silica is a material of choice in numerous applications thanks to its large porosity, specific surface area, and tunable pore size.[1,2] Indeed, mesoporous silica has been used in catalysis,[1,2] photocatalysis,[3] separation,[4] low-k dielectrics,[5] and biomedical applications,[6–8] to name a few. One of the most notable applications is thermal insulation applications.[9] For example, silica aerogels feature porosity above 70% and specific surface area larger than $1000\,m^2\,g^{-1}$, resulting in an extremely low thermal conductivity around $0.013\,W\,m^{-1}\,K^{-1}$ under ambient conditions.[9]

The accurate measurement of such a low thermal conductivity is challenging. Time-domain thermoreflectance (TDTR) is a transient method suited to measure the thermal conductivity of aerogels or other mesoporous materials from thermal effusivity measurements defined as[10]

$$e = \sqrt{k_{eff}(\rho c_p)_{eff}}, \tag{1}$$

where k_{eff} is the effective thermal conductivity and $(\rho c_p)_{eff}$ is the effective volumetric heat capacity. Similarly, the laser flash method measures the effective thermal diffusivity[11]

$$\alpha = k_{eff}/(\rho c_p)_{eff}. \tag{2}$$

In both methods, retrieving the effective thermal conductivity requires prior knowledge of the effective volumetric heat capacity defined as

$$(\rho c_p)_{eff} = \rho_{eff} c_{p,eff}, \tag{3}$$

where ρ_{eff} is the effective density and $c_{p,eff}$ is the effective specific heat capacity. It is common to assume that the effective volumetric heat capacity $(\rho c_p)_{eff}$ of aerogel, and porous media in general, is equal to the volume-fraction-weighted sum of the volumetric heat capacity of bulk silica and air expressed as[10]

$$\begin{aligned}(\rho c_p)_{eff} &= \phi(\rho c_p)_{air} + (1-\phi)(\rho c_p)_{SiO_2} \\ &\approx (1-\phi)\rho_{SiO_2} c_{p,SiO_2},\end{aligned} \tag{4}$$

where ϕ is the porosity, while $(\rho c_p)_{air}$ and $(\rho c_p)_{SiO_2}$ are the volumetric heat capacity of air and bulk silica, respectively. Typically, the contribution of air is neglected as $(\rho c_p)_{air} \ll (\rho c_p)_{SiO_2}$. Similarly, calorimetric measurements of phase transitions of mesopore-confined matter in mesoporous silica assumed the effective specific heat capacity of mesoporous silica as that of bulk silica.[12]

At room temperature, there are on average 4.9 OH groups per nm^2 on the surface of amorphous silica.[13] The amount of surface OH groups depends on previous heat treatment. At high temperature, surface OH groups undergo co-condensation reaction according to[14]

$$\text{Si–OH} + \text{Si–OH} = \text{Si–O–Si} + \text{H}_2\text{O}. \tag{5}$$

Note that here only the reacting bonds are shown. The co-condensation reaction can reduce the surface density of OH groups σ_{OH} down to 0.2 OH nm^{-2} at 1000 °C.[13] As any chemical reaction, however, reaction (5) tends toward equilibrium at a given temperature. As a result, any high-temperature treatment of mesoporous silica can remove surface OH groups only temporarily because they regenerate

a)Author to whom correspondence should be addressed: pilon@seas.ucla.edu

over time when the material cools to room temperature in the presence of water or humidity. Moreover, the contribution of surface groups to the heat capacity may be magnified by the large specific surface area characteristics of mesoporous silica, often exceeding 1000 $m^2\ g^{-1}$.

The present study aims to elucidate the effect of surface OH groups on the effective specific $c_{p,eff}$ and volumetric $(\rho c_p)_{eff}$ heat capacity of mesoporous silica with various morphologies. To do so, the specific surface area S_a, porosity ϕ, effective specific heat capacity $c_{p,eff}$, and effective density ρ_{eff} of a wide variety of mesoporous silica samples were measured independently. In addition, a thermodynamic model was developed based on surface energy considerations to account for the effect of surface OH groups on the effective specific and volumetric heat capacity.

Twelve different mesoporous silica samples were prepared including (a) two mesoporous nanoparticle-based powders S1 and S2, (b) two mesoporous sol-gel powders S3 and S4, and (c) eight mesoporous ambigel silica samples S5–S12 dried by solvent exchange at room temperature.[15] Different synthesis methods were used to ensure structural diversity of the investigated materials.

Mesoporous nanoparticle-based silica sample S1 was prepared by dissolving 0.452 g of triblock copolymer Pluronic P123 ($EO_{20}PO_{70}EO_{20}$, M = 5750 Da, BASF, Florham Park, NJ, USA) in 2 ml of deionized water at room temperature. Next, 2 ml of an aqueous suspension of SiO_2 nanoparticles (Nalco 2326, 15 wt. %, ammonia-stabilized colloidal silica nanoparticles 5 nm in diameter, Nalco Chemical Company, Naperville, IL, USA) was added, and the resulting solution was stirred at room temperature for 3 h to ensure sufficient mixing. The solution was then poured into a Petri dish, evaporated, and dried for 7 days. The resulting powder was calcined in a tube furnace under flowing O_2 using the following temperature program: (1) temperature was raised from room temperature to 180 °C using a 1.33 °C min^{-1} heat ramp and held for 4 h; (2) temperature was raised to 400 °C using a 2 °C min^{-1} heat ramp and held for 3 h; (3) the furnace was allowed to free cool down to room temperature. The temperature program was designed to ensure full polymer removal and to minimize changes in the mesoporous structure at high temperatures.[16–18] Mesoporous nanoparticle-based silica sample S2 was prepared by evaporating 5 ml of the SiO_2 nanoparticle solution in a Petri dish, drying the resulting powder for 5 days, and calcining using the same procedure as for sample S1.

Mesoporous sol-gel silica sample S3 was prepared by mixing 0.634 ml of tetraethyl orthosilicate (98%, Acros Organics, NJ, USA), 1.66 ml of 0.05 M aqueous HCl (certified ACS Plus, Fisher Scientific, Pittsburgh, PA, USA), 6.21 ml of ethanol (200 proof, Rossville Gold Shield, Hayward, CA, USA), and 0.26 g of triblock copolymer Pluronic P123 at room temperature for 10 min to ensure sufficient mixing. The solution was then poured into a Petri dish, evaporated, and dried for 7 days. The resulting powder was then calcined using the same procedure as for samples S1 and S2. Mesoporous sol-gel silica sample S4 was prepared according to the same procedure as sample S3 but using 0.102 g of triblock copolymer Pluronic P123.

Silica ambigel samples S5–S12 were prepared according to the previously reported recipe.[15] Briefly, tetraethyl orthosilicate (Sigma-Aldrich, St. Louis, MO, USA), ethanol (Decon Labs, Inc., King of Prussia, PA, USA), deionized water, formamide (Sigma-Aldrich, St. Louis, MO, USA), and HCl (37 wt. % in water, Sigma-Aldrich, St. Louis, MO, USA) were mixed together at molar ratios of $1:2:4:1:3.8\times10^{-2}$ (S5 and S9–S11), $1:3:4:0.5:3.8\times10^{-2}$ (S6), $1:2:8.5:0.5:3.8\times10^{-2}$ (S7), and $1:1:4:1:3.8\times10^{-2}$ (S8). In the case of ambigel sample S12, tetramethyl orthosilicate (Sigma-Aldrich, St. Louis, MO, USA), deionized water, and HCl were mixed at a molar ratio of $1:12:1.6\times10^{-4}$. The resulting solution was stirred for 2 h before transferring into a 10 cm × 10 cm × 1 mm plastic mold for gelation, followed by aging for 2 days (S9), 6 days (S5–S8, S10, and S12), or 8 days (S11) at room temperature. The gel was then removed from the mold, and the aqueous solution filling the pores was exchanged with acetone (Sigma-Aldrich, St. Louis, MO, USA) six times over two days at room temperature, followed by acetone exchange with cyclohexane (Sigma-Aldrich, St. Louis, MO, USA) six times over two additional days at room temperature. The gel was then dried in a cyclohexane-rich atmosphere at room temperature for a week. Finally, the gel was calcined in a box furnace in static air using the following temperature program: (1) temperature was raised from room temperature to 500 °C using a 1 °C min^{-1} heat ramp and held for 24 h; (2) the furnace was cooled down to room temperature using a 1 °C min^{-1} temperature ramp.

The prepared mesoporous SiO_2 samples were characterized by (i) low-temperature nitrogen adsorption–desorption isotherms, (ii) Fourier-transform infrared (FTIR) spectroscopy, (iii) powder X-ray diffraction (XRD), and (iv) differential scanning calorimetry (DSC). All details of these measurements and calculations are provided in the supplementary material. Nitrogen porosimetry provided the specific surface area S_a, total pore volume V_t, porosity ϕ, micropore volume V_{mi}, and average pore width $\overline{d}_p$. FTIR and powder XRD were used to establish the chemical composition and crystallinity of the samples. DSC measurements provided the effective specific heat capacity $c_{p,eff}$ and water weight fraction w_{H2O}.

Table I summarizes the measured structural properties of all the prepared mesoporous silica samples. The nanoparticle-based porous silica samples S1 and S2 were exclusively mesoporous, i.e., their average pore width $\overline{d}_p$ was between 2 and 50 nm. They had the smallest specific surface area S_a

TABLE I. Structural properties of all the prepared mesoporous silica samples.

Sample	Type	S_a ($m^2\ g^{-1}$)	V_t ($cm^3\ g^{-1}$)	V_{mi} ($cm^3\ g^{-1}$)	ϕ (%)	$\overline{d}_p$ (nm)
S1	Nanoparticles	260	0.77	0.00	63	12.3
S2	Nanoparticles	350	0.35	0.00	44	4.9
S3	Sol-gel	440	0.43	0.07	49	5.4
S4	Sol-gel	390	0.22	0.13	32	3.5
S5	Ambigel	700	0.45	0.03	50	3.7
S6	Ambigel	520	0.30	0.07	40	3.4
S7	Ambigel	1000	0.59	0.15	56	3.4
S8	Ambigel	570	0.35	0.05	43	2.2
S9	Ambigel	550	0.40	0.02	47	2.8
S10	Ambigel	700	0.46	0.03	50	2.3
S11	Ambigel	680	0.52	0.04	53	2.2
S12	Ambigel	510	0.34	0.03	43	3.8

(260–350 $m^2\ g^{-1}$) but the largest porosity ϕ (44%–63%) and average pore width $\overline{d}_p$ of 4.9–12.3 nm. In addition to mesopores, the sol-gel silica samples S3 and S4 and ambigel samples S5–S12 also featured a small fraction of micropores (pore width < 2 nm). The sol-gel silica samples S3 and S4 featured specific surface area S_a in the range of 390–440 $m^2\ g^{-1}$, while ambigel samples S5–S12 had the largest specific surface area S_a of all samples (510–1000 $m^2\ g^{-1}$). The sol-gel silica and ambigel samples had porosity ϕ between 32% and 56%. The sol-gel silica samples had the average pore width $\overline{d}_p$ of 3.5–5.4 nm, while ambigels had the smallest average pore width $\overline{d}_p$ of all samples (2.2–3.8 nm).

All FTIR spectra of representative nanoparticle-based, sol-gel, and ambigel mesoporous silica samples (Fig. S1 in the supplementary material) featured a broad absorption band between 3700 and 3000 cm^{-1} corresponding to O–H stretching vibrations of OH surface groups and OH groups in water physically adsorbed on the materials' surface.[19–21] In addition, all samples featured an absorption band in the range of 1630–1620 cm^{-1} corresponding to H–O–H bending vibrations of physisorbed water.[19–21] Multiple absorption bands at 1200–1000, 970–940, 800, 580–550, and 470–450 cm^{-1} were all ascribed to vibrations of the SiO_2 network: Si–O–Si asymmetric stretching, Si–OH in-plane stretching, Si–O symmetric stretching, Si–O stretching, and O–Si–O bending vibrations, respectively.[19–21] Finally, no absorption bands in the range of 3000–1350 cm^{-1}, corresponding to organic molecules, were detected. Therefore, the prepared samples did not contain organic residues that could otherwise affect the measured effective specific heat capacity $c_{p,eff}$. In addition, X-ray diffraction patterns of the same selected mesoporous silica samples (Fig. S2 in the supplementary material) were featureless except for a broad hump between 2θ equal to 10° and 40°, indicating that the mesoporous SiO_2 samples were amorphous.[22]

Table II summarizes the experimental measurements of specific heat capacity $c_{p,eff}$ of degassed mesoporous silica samples. As a result of their large specific surface area S_a, the investigated mesoporous silica samples contained w_{H_2O} = 3–17 wt. % of physically adsorbed water after equilibration with ambient air.

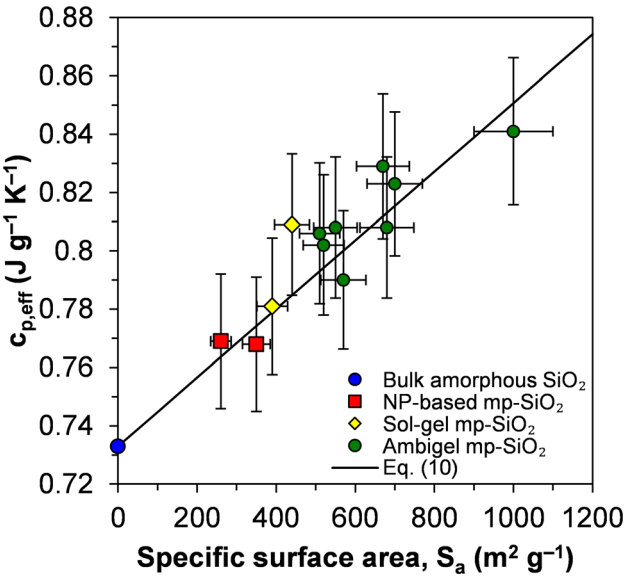

FIG. 1. Effective specific heat capacity $c_{p,eff}$ of all investigated mesoporous silica samples as a function of specific surface area S_a. The black line represents $c_{p,eff}$ predicted using Eq. (10). The horizontal error bars represent 10% experimental uncertainty of S_a, and the vertical error bars represent 3% experimental uncertainty of $c_{p,eff}$. NP-based and mp-SiO_2 stand for nanoparticle-based and mesoporous SiO_2, respectively.

Figure 1 shows the effective specific heat capacity $c_{p,eff}$ as a function of specific surface area S_a measured for all samples. It indicates that $c_{p,eff}$ was systematically larger than that of bulk amorphous silica, which has a reported value of 0.733 J g^{-1} K^{-1}.[23] The deviations from bulk behavior were 5%–13%, while the experimental uncertainty was less than 3%. In addition, Fig. 1 shows that the effective specific heat capacity $c_{p,eff}$ of mesoporous silica increased almost linearly with increasing specific surface area S_a. The linear dependence was attributed to the contribution of OH groups present on the surface of the investigated samples.

In general, the effective specific heat capacity $c_{p,eff}$ (in J g^{-1} K^{-1}) of a material made of N constituents can be calculated as a weight-fraction-average of all contributing phases[24]

TABLE II. Water weight fraction and experimental and predicted effective specific and volumetric heat capacity of all the prepared mesoporous silica samples.[a]

		$c_{p,eff}$ (J g^{-1} K^{-1})			$(\rho c_p)_{eff}$ (10^6 J m^{-3} K^{-1})		
Sample	w_{H_2O} (%)	Exp.	Bulk SiO_2	Eq. (10)	Exp.	Eq. (4)	Eq. (12) ($\overline{d}_p$ = exp.)
S1	4.6	0.769	0.733 (5%)	0.764 (0.7%)	0.626	0.597 (5%)	0.621 (0.8%)
S2	5.0	0.768	0.733 (5%)	0.774 (0.8%)	0.946	0.903 (5%)	0.945 (0.1%)
S3	12.3	0.809	0.733 (9%)	0.784 (3.1%)	0.908	0.822 (9%)	0.865 (4.7%)
S4	3.2	0.781	0.733 (6%)	0.779 (0.3%)	1.17	1.10 (6%)	1.14 (2.6%)
S5	15.6	0.823	0.733 (11%)	0.815 (1.0%)	0.905	0.806 (11%)	0.870 (3.9%)
S6	16.7	0.802	0.733 (9%)	0.794 (1.0%)	1.06	0.968 (9%)	1.02 (3.8%)
S7	16.3	0.841	0.733 (13%)	0.853 (1.4%)	0.814	0.710 (13%)	0.787 (3.3%)
S8	16.3	0.790	0.733 (7%)	0.800 (1.3%)	0.991	0.919 (7%)	1.01 (1.9%)
S9	7.1	0.808	0.733 (9%)	0.798 (1.2%)	0.942	0.855 (9%)	0.934 (0.8%)
S10	8.8	0.829	0.733 (12%)	0.815 (1.7%)	0.912	0.806 (12%)	0.909 (0.3%)
S11	5.0	0.808	0.733 (9%)	0.813 (0.6%)	0.835	0.758 (9%)	0.871 (4.3%)
S12	17.4	0.806	0.733 (9%)	0.793 (1.6%)	1.01	0.919 (9%)	0.972 (3.8%)

[a]exp.—denotes experimental; values in parentheses represent the relative difference from the respective experimental values.

$$c_{p,eff} = \sum_{i=1}^{N} w_i c_{p,i}, \tag{6}$$

where w_i and $c_{p,i}$ are the weight fraction and the specific heat capacity of constituent i. In the case of mesoporous silica with pore surface supporting OH groups, Eq. (6) simplifies to

$$\begin{aligned} c_{p,eff} &= w_{SiO_2} c_{p,SiO_2} + w_{OH} c_{p,OH} + w_{air} c_{p,air} \\ &\approx w_{SiO_2} c_{p,SiO_2} + w_{OH} c_{p,OH}, \end{aligned} \tag{7}$$

where subscript SiO_2, OH, and air refer to silica, OH groups, and air, respectively. Here also, the contribution of air to $c_{p,eff}$ was negligibly small because the weight fraction of air is very small, i.e., $w_{air} \ll 0.01$. By definition, the sum of all weight fractions is equal to unity, i.e.,

$$1 = w_{SiO_2} + w_{OH} + w_{air} \approx w_{SiO_2} + w_{OH} = \frac{m_{SiO_2}}{m_{total}} + \frac{m_{OH}}{m_{total}}, \tag{8}$$

where m_{SiO_2}, m_{OH}, and m_{total} ($= m_{SiO_2} + m_{OH}$) are the mass of silica, surface OH groups, and the total sample, respectively. The mass of OH groups m_{OH} (in g) can be expressed as

$$m_{OH} = M_{OH} n_{OH} = M_{OH} \sigma_{OH} S_a m_{total}, \tag{9}$$

where M_{OH} is the molar mass of OH groups ($M_{OH} = 17$ g mol^{-1}), n_{OH} is the number of moles of OH groups (in mol), σ_{OH} is the surface density of OH groups (in mol m^{-2}), and S_a is the specific surface area of the mesoporous silica sample (in m^2 per total mass of the sample). Combining Eqs. (7)–(9) yields

$$c_{p,eff} = c_{p,SiO_2} + M_{OH} \sigma_{OH} S_a (c_{p,OH} - c_{p,SiO_2}). \tag{10}$$

Equation (10) indicates that the effective heat capacity $c_{p,eff}$ of mesoporous silica is directly proportional to the specific surface area S_a as shown in Fig. 1. The specific heat capacity $c_{p,OH}$ of OH groups can be estimated using the group contributions theory.[25] Thus, the molar heat capacity of the OH group was estimated to be 26.9 J mol^{-1} K^{-1},[25] corresponding to a specific heat capacity $c_{p,OH}$ of 1.58 J g^{-1} K^{-1}. In other words, OH groups feature a much larger specific heat capacity than bulk amorphous silica (0.733 J g^{-1} K^{-1}).[23] Thus, the presence of surface OH groups can have a significant impact on the effective specific heat capacity $c_{p,eff}$ of mesoporous silica. Also note that if silica has a negligibly small specific surface area S_a or a small surface density of OH groups σ_{OH}, the effective heat capacity approaches that of bulk silica.

Table II summarizes the effective specific heat capacity $c_{p,eff}$ predicted by Eq. (10) for all mesoporous silica samples investigated. Figure 1 also shows the predictions of $c_{p,eff}$ by Eq. (10) as a function of specific surface area S_a, assuming $c_{p,SiO_2} = 0.733$ J g^{-1} K^{-1},[23] $c_{p,OH} = 1.58$ J g^{-1} K^{-1},[25] and $\sigma_{OH} = 4.9$ OH nm^{-2}.[13] Excellent agreement was obtained with experimental measurements. In fact, the predicted linear dependence fit all the data points within the experimental uncertainty. Slight deviations for some samples, especially the mesoporous sol-gel silica, were probably due to higher than average surface density of OH groups σ_{OH}.[13] Overall, the proposed model accurately described the experimentally measured effective specific heat capacity $c_{p,eff}$ of mesoporous silica. Note that for mesoporous silica with $S_a = 1000$ m^2 g^{-1}, the effective specific heat capacity would be $c_{p,eff} = 0.85$ J g^{-1} K^{-1}, i.e., 16% larger than that of bulk silica.[23]

To account for the contribution of surface OH groups to the effective volumetric heat capacity $(\rho c_p)_{eff}$ of mesoporous silica in Eq. (4), the effective specific heat capacity $c_{p,eff}$ of mesoporous silica can be substituted by Eq. (10) as follows:

$$(\rho c_p)_{eff} = (1-\phi)\rho_{SiO_2}\left[c_{p,SiO_2} + M_{OH}\sigma_{OH}S_a(c_{p,OH} - c_{p,SiO_2})\right]. \tag{11}$$

Substituting V_t and S_a, given by Eqs. (S1) and (S3) in the supplementary material, into Eq. (11) yields

$$(\rho c_p)_{eff} = (1-\phi)\rho_{SiO_2}\left[c_{p,SiO_2} + 4\frac{\phi}{(1-\phi)\rho_{SiO_2}} \times \frac{M_{OH}\sigma_{OH}}{\overline{d}_p}(c_{p,OH} - c_{p,SiO_2})\right]. \tag{12}$$

Figure 2 compares the effective volumetric heat capacity $(\rho c_p)_{eff}$ of the investigated mesoporous silica samples measured experimentally as a function of porosity ϕ and predicted by Eqs. (4) and (12) with $\rho_{SiO_2} = 2.2$ g cm^{-3}.[26] The latter calculation assumed an average pore width $\overline{d}_p$ of either 2 or 10 nm, corresponding to the lower and upper bounds of $\overline{d}_p$ in the investigated mesoporous silica samples. Figure 2 shows that the measured effective volumetric heat capacity $(\rho c_p)_{eff}$ was larger than the predictions by the conventional volume-fraction-weighted model [Eq. (4)] by 5%–13%. By

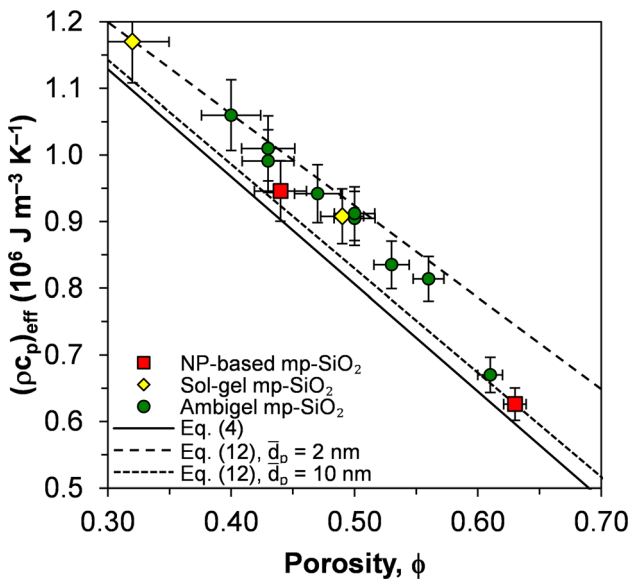

FIG. 2. Effective volumetric heat capacity $(\rho c_p)_{eff}$ of all investigated silica samples as a function of porosity ϕ. The solid black line represents $(\rho c_p)_{eff}$ predicted without the surface OH groups' contribution using Eq. (4). The dashed black lines represent $(\rho c_p)_{eff}$ predicted with the surface OH groups' contribution using Eq. (12) (assuming average pore widths $\overline{d}_p$ of 2 and 10 nm). The horizontal error bars represent an experimental uncertainty of 0.03 cm^3 g^{-1} in V_t propagated to ϕ, and the vertical error bars represent combined uncertainty in ϕ and 3% uncertainty in $c_{p,eff}$. NP-based and mp-SiO_2 stand for nanoparticle-based and mesoporous SiO_2, respectively.

contrast, predictions by Eq. (12) fell within 0.1%–4.7% of the measured volumetric heat capacity $(\rho c_p)_{eff}$ (see Table II).

To conclude, this paper elucidated the effect of surface hydroxyl groups on the effective specific and volumetric heat capacities of mesoporous silica. The investigated mesoporous silica samples were prepared using different synthetic methods to achieve a wide range of porosities, specific surface area, and pore size. The experimental specific and volumetric heat capacities were larger than the corresponding weight-fraction-weighted specific heat capacity and volume-fraction-weighted volumetric heat capacity of the constituents. The discrepancy was attributed to the presence of OH groups on the surface of the investigated mesoporous silica samples. A thermodynamic model based on surface energy considerations was developed to account for the effect of surface OH groups on the specific and volumetric heat capacities. The model predicted the experimental specific and volumetric heat capacities within 1%–4%. By contrast, neglecting the effect of surface OH groups resulted in inaccurate specific and volumetric heat capacities. Finally, a similar effect of surface groups on specific and volumetric heat capacities should be considered in other mesoporous materials with a large surface area.[27,28]

See supplementary material for the nomenclature and the details on the measurements of total pore volume, porosity, micropore volume, specific surface area, average pore width, specific heat, water weight fraction, FTIR transmission spectra, and XRD patterns.

This research was supported in part by Advanced Research Projects Agency-Energy (ARPA-E) Single-Pane Highly Insulating Efficient Lucid Designs (SHIELD) program (ARPA-E Award No. DE-AR0000738). The authors are grateful to BASF (Florham Park, NJ, USA) and Nalco Chemical Company (Naperville, IL, USA) for generously providing triblock copolymer Pluronic P123 and an aqueous suspension of SiO_2 nanoparticles Nalco 2326, respectively.

[1]A. Corma, Chem. Rev. **97**, 2373 (1997).
[2]F. Hoffmann, M. Cornelius, J. Morell, and M. Fröba, Angew. Chem., Int. Ed. **45**, 3216 (2006).
[3]M. Anpo and M. Takeuchi, J. Catal. **216**, 505 (2003).
[4]K. Moller and T. Bein, Chem. Mater. **10**, 2950 (1998).
[5]M. E. Davis, Nature **417**, 813 (2002).
[6]M. Hartmann, Chem. Mater. **17**, 4577 (2005).
[7]M. Vallet-Regí, F. Balas, and D. Arcos, Angew. Chem., Int. Ed. **46**, 7548 (2007).
[8]I. Slowing, J. Viveroescoto, C. Wu, and V. Lin, Adv. Drug Delivery Rev. **60**, 1278 (2008).
[9]R. Baetens, B. P. Jelle, and A. Gustavsen, Energy Build. **43**, 761 (2011).
[10]P. E. Hopkins, B. Kaehr, E. S. Piekos, D. Dunphy, and C. J. Brinker, J. Appl. Phys. **111**, 113532 (2012).
[11]W. J. Parker, R. J. Jenkins, C. P. Butler, and G. L. Abbott, J. Appl. Phys. **32**, 1679 (1961).
[12]C. Schaefer, T. Hofmann, D. Wallacher, P. Huber, and K. Knorr, Phys. Rev. Lett. **100**, 175701 (2008).
[13]L. T. Zhuravlev, Langmuir **3**, 316 (1987).
[14]C. J. Brinker and G. W. Scherer, *Sol-Gel Science: The Physics and Chemistry of Sol-Gel Processing* (Academic Press, Boston, 1990).
[15]J. H. Harreld, W. Dong, and B. Dunn, Mater. Res. Bull. **33**, 561 (1998).
[16]F. Bérubé and S. Kaliaguine, Microporous Mesoporous Mater. **115**, 469 (2008).
[17]D. Zhao, Q. Huo, J. Feng, B. F. Chmelka, and G. D. Stucky, J. Am. Chem. Soc. **120**, 6024 (1998).
[18]D. Zhao, J. Feng, Q. Huo, N. Melosh, G. H. Fredrickson, B. F. Chmelka, and G. D. Stucky, Science **279**, 548 (1998).
[19]R. F. S. Lenza and W. L. Vasconcelos, Mater. Res. **4**, 189 (2001).
[20]R. Al-Oweini and H. El-Rassy, J. Mol. Struct. **919**, 140 (2009).
[21]C. Knöfel, C. Martin, V. Hornebecq, and P. L. Llewellyn, J. Phys. Chem. C **113**, 21726 (2009).
[22]H. Hamdan, M. N. M. Muhid, S. Endud, E. Listiorini, and Z. Ramli, J. Non-Cryst. Solids **211**, 126 (1997).
[23]P. Richet, Y. Bottinga, L. Denielou, J. P. Petitet, and C. Tequi, Geochim. Cosmochim. Acta **46**, 2639 (1982).
[24]J. R. Howell and R. O. Buckius, *Fundamentals of Engineering Thermodynamics*, English/SI version (McGraw-Hill Book Co, New York, 1987).
[25]D. N. Rihani and L. K. Doraiswamy, Ind. Eng. Chem. Fundam. **4**, 17 (1965).
[26]*CRC Handbook of Chemistry and Physics*, edited by J. R. Rumble, 98th ed. (CRC Press, Taylor & Francis Group, Boca Raton, London, New York, 2017).
[27]J. Fang and L. Pilon, Appl. Phys. Lett. **101**, 011909 (2012).
[28]P. Huber, J. Phys.: Condens. Matter **27**, 103102 (2015).